Open problems in liquids dynamics: the role of neutron scattering

Eleonora Guarini[1*], *Gianmarco* Masini[1], *Ubaldo* Bafile[2], *Milva* Celli[2], *Daniele* Colognesi[2], *Alessandro* Cunsolo[3], *Luisa* Scaccia[4], *Alessio* De Francesco[5], and *Ferdinando* Formisano[5]

[1]Dipartimento di Fisica e Astronomia, Università degli Studi di Firenze, I-50019 Sesto Fiorentino, Italy
[2]Consiglio Nazionale delle Ricerche, Istituto di Fisica Applicata "Nello Carrara", I-50019 Sesto Fiorentino, Italy
[3]Department of Physics, University of Wisconsin-Madison, Madison, WI 53706, United States
[4]Dipartimento di Economia e Diritto, Università di Macerata, I-62100 Macerata, Italy
[5]CNR-IOM & INSIDE@ILL c/o Operative Group in Grenoble and Institut Laue Langevin, F-38042 Grenoble, France

Abstract. We review recent inelastic neutron scattering experiments aimed at investigating still open issues in the microscopic dynamics of liquids. It is shown that the interpretation of experimental results is put on solid ground by the application of modern methods of analysis and lineshape modelling which ensure the fulfillment of fundamental physical properties that the spectra must obey. This last condition becomes crucial to avoid overinterpretations of the genuine information conveyed by scattering data, especially when studying weak signals in the dynamic structure factor. Moreover, we highlight the different roles that neutron data presently play compared to molecular dynamics simulations depending on the nature of the sample, including the case of quantum liquids. In particular, we show how neutron measurements remain an indispensable benchmark in assessing the present capabilities of classical and quantum simulation methods. We also mention the potential of statistical methods, such as Bayesian inference, when applied to neutron data analysis and the opportunity they provide in establishing the spectral features without arbitrary assumptions on the model lineshape.

1 Introduction

Inelastic neutron scattering (INS) is a master technique for experimental studies on the dynamic behaviour, at the nanometre and picosecond scales, of various classes of liquids. Topical examples are given by the pioneering works on the longitudinal collective excitations (sound waves) in liquid metals as Pb and Rb [1,2], which opened the way to the numerous investigations on metallic liquids carried out up to present times [3,4]. In particular, these simple monatomic liquids were more recently taken as reference systems for studies of shear waves through the search for possible low frequency excitations in the dynamic structure factor $S(Q,\omega)$ [5], which is accessed by both INS and inelastic x-ray scattering (IXS) techniques when the probe exchanges a momentum $\hbar\mathbf{Q}$ and an energy $E = \hbar\omega$ with the sample, $\hbar$ being the reduced Planck constant.

However, the true realm of neutron scattering is liquid H_2, together with its heavier counterpart D_2. Across the years, both these fluids attracted much interest when investigating general aspects of the single-particle (self) dynamics of an incoherent scatterer like H_2 [6-9], or quantum effects on either the self [10,11] or the collective properties [12-14] of these systems. In fact, the low molecular mass of H_2 and D_2 and the low temperatures at which they are in the liquid phase lead to evident manifestations of quantum behaviour, as further detailed in Sect. 3. Moreover, H_2 and D_2 are the most used moderating materials for the production of low-energy (about 1 meV) neutrons. In this respect, the design of new generation hydrogen-based cold neutron sources requires the availability of reliable databases of the scattering law taking explicitly the quantum nature of these fluids into account. Simultaneously, it demands an efficient mapping of the whole kinematic (Q,ω) range for best estimates of the response function. Such requirements unavoidably call for simulation methods capable of providing reliable dynamical data on H_2 and D_2, since experiments will never cover, in reasonable times, the innumerable kinematic conditions contributing to a total cross section calculation, with varying incident neutron energy. Available semiclassical methods for simulating the dynamics of H_2 and D_2, like ring polymer molecular dynamics (RPMD) [15] and two versions of the Feynman-Kleinert (FK) approach [16,17], urge then an experimental check, and neutrons are the best probe for this purpose.

Here we review recent INS investigations of both the mentioned classes of liquids, with specific interest in the methods of analysis. In particular, we first address the case of liquids which can be assumed to behave classically, like molten metals, with special focus on the still debated claim that the experimental $S(Q,\omega)$ of some metals [18,19] bears the signature of low-frequency transverse-like excitations. As a matter of fact, a

* Corresponding author: guarini@fi.infn.it

dependence on the methods of analysis emerges, so the state of the art of reliable approaches for model fitting to the data is discussed in some detail.

The remainder of the paper deals with the case of a quantum liquid like D_2, while discussing the present need for absolute scale comparisons between neutron data and quantum simulations probing the translational dynamics through the centre of mass dynamic structure factor $S_{CM}(Q,\omega)$ of the liquid. Indeed, the effectiveness of quantum calculations of the microscopic dynamics has been poorly tested until present, hindering the possible use of existing quantum simulation methods in the mentioned applications related to cold neutron production. The benchmark of neutron measurements evidences the still lacking performance of the semiclassical approximations adopted in each of the available quantum simulation techniques.

2 Transverse dynamics of liquid metals

In the 1970s, simulation studies of specific time autocorrelation functions [20] have shown that dense fluids can sustain shear wave propagation at sufficiently small wavelengths (around and below 0.5 nm, approximately). The specific functions we are referring to are the transverse current autocorrelation function $C_T(Q,t)$ and the velocity autocorrelation function $Z(t)$. The former is given by

$$C_T(Q,t) = \langle \mathbf{j}_T^*(\mathbf{Q},0) \cdot \mathbf{j}_T(\mathbf{Q},t) \rangle / (2N), \quad (1)$$

with $\mathbf{j}_T(\mathbf{Q},t) = \mathbf{j}(\mathbf{Q},t) - \mathbf{j}_L(\mathbf{Q},t)$, where the current of an N particle system is $\mathbf{j}(\mathbf{Q},t) = \sum_\alpha \mathbf{v}_\alpha(t) \exp[i\,\mathbf{Q} \cdot \mathbf{R}_\alpha(t)]$, $\mathbf{R}_\alpha(t)$ and $\mathbf{v}_\alpha(t)$ denoting the position and velocity of the α-th particle at time t, and $\mathbf{j}_L(\mathbf{Q},t)$ is the longitudinal current, i.e. the projection of $\mathbf{j}(\mathbf{Q},t)$ on the wavevector $\mathbf{Q}$. The angular brackets in Eq. (1) stand for the statistical average in the canonical ensemble [5]. The velocity autocorrelation function is defined by

$$Z(t) = \sum_\alpha \langle \mathbf{v}_\alpha(0) \cdot \mathbf{v}_\alpha(t) \rangle / N. \quad (2)$$

In particular, the spectrum $Z(\omega)$ of Eq. (2) can be considered, for a liquid, as a sort of equivalent of the phonon density of states (DoS) in solid state physics. Unfortunately, neither $Z(\omega)$, nor the spectrum of the transverse current autocorrelation function, $C_T(Q,\omega)$, can actually be measured. Indeed, past determinations of $Z(\omega)$ by incoherent neutron scattering [6-8] revealed to be demanding. INS and IXS experiments enable the determination of the space and time Fourier transform of the microscopic density autocorrelation function, i.e. of the dynamic structure factor $S(Q,\omega)$ mentioned in the Introduction. However, $S(Q,\omega)$ is a longitudinal quantity by definition [5], therefore detectability of transverse-like contributions to this function has often been objected as a matter of principle [21]. Nonetheless, more than ten years ago, at least two papers analyzing IXS data on two molten metals [18,19] reported the presence of an additional low-frequency component in the measured $S(Q,\omega)$. In both works, the same phenomenological model was fitted to the experimental spectra. In particular, the fit function was modelled by adding one or two (depending on Q) damped harmonic oscillator (DHO) doublets [22] to a central Lorentzian, the latter accounting for relaxation processes in an effective way. However, such a modelling disregards the fact that the global fit function has a divergent second frequency moment [5,22] in place of the finite theoretical value $k_B T Q^2 / M$, where k_B is Boltzmann constant, T the temperature, and M the atomic mass of the fluid. As we will show, the physical consistency of the adopted models can instead be decisive for a correct interpretation of the experimental results.

At present, there are two possibilities to limit the arbitrariness of fit-based procedures. The first is based on the availability of an exact theory for the functional form of autocorrelation functions and corresponding spectra [23-25], where known constraints can be easily imposed. In this case, one can choose a few tentative models guided by physical considerations, then enforce at least the most important sum rules that $S(Q,\omega)$ must obey, and finally check which model provides the best fit quality with simultaneous minimization of the number of free parameters.

The other possibility is to control model fitting to the data on a statistical basis, without imposing *a priori* the number of excitations. At present, we use simple phenomenological models in a complex algorithm exploiting Bayes theorem to estimate the posterior probabilities, conditional to the experimental data, of the various parameters, including the number of excitations itself [26]. The information from the posterior distributions permits to control, in a statistical sense, what the data actually support.

Both the theoretically and the probabilistically grounded approaches for the modelling of the scattering signal are briefly described in the next subsections.

2.1 Exponential Expansion Theory (EET)

The theory states that any normalized autocorrelation function $c(t) / c(0) = \langle A(0)\, A(t) \rangle / \langle A(0)^2 \rangle$ of a generic dynamical variable $A(t)$ can be represented by a series of exponential terms, called *modes*, with generally complex amplitudes I_j and frequencies z_j, i.e.:

$$c(t) / c(0) = \sum_j I_j \exp(z_j \mid t \mid). \quad (3)$$

Consequently, the spectrum is a sum of so-called generalized Lorentzian lines

$$c(\omega) / c(t = 0) = \sum_j (-I_j z_j) / [\pi (\omega^2 + z_j^2)]. \quad (4)$$

In particular, if I_j and z_j are real, we are dealing with relaxation processes with decay constant $z_j < 0$, which contribute with genuine central Lorentzians to the spectrum. If I_j and z_j are complex, pairs of conjugate modes are present in the series and account for damped oscillatory components in the correlation function due to collective excitations characterized by a damping $\mathrm{Re}(z_j) < 0$ and a frequency $\mathrm{Im}(z_j)$. Such complex pairs correspond to two distorted Lorentzian lines in the spectrum, centred at the nonzero frequencies $\pm\,\mathrm{Im}(z_j)$, respectively. As far as the sum rules are concerned,

normalization is guaranteed by enforcing the condition $\sum_j I_j = 1$. In addition, constraints are imposed on the odd time derivatives of $c(t)$ at $t = 0$ in the form

$$[d^p c(t) / dt^p]_{t=0} = \sum_j I_j z_j^p = 0, \text{ for odd } p \qquad (5)$$

which ensure the correct behaviour of the function at the time origin and are equivalent to require the finiteness of the even spectral moments in the frequency domain.

Luckily, most correlation functions of interest in liquids dynamics are accurately described by a small number of modes, meaning that the main dynamical processes are actually few. The scheme of the modes may of course change with varying the thermodynamic state and the probed length scale (Q). At each wavevector and thermodynamic state, the best model is chosen on the basis of the corresponding fit quality and of some general knowledge on liquids' behaviour.

In what follows, three models complying with the general EET will be considered for $S(Q,\omega)$. The simpler one is a generalized hydrodynamics (GH) triplet with Q-dependent parameters [5]. It is a single-excitation model consisting of one central Lorentzian, accounting for thermal diffusion and structural relaxation in an effective way, plus one doublet of distorted Lorentzians representing the longitudinal sound waves propagating in the fluid. The model spectrum is constrained to have a finite second frequency moment. The second modelling is the viscoelastic (VE) lineshape [22], which differs from the GH one as regards the relaxation phenomena (two central Lorentzians in place of a single one) and the obeyed sum rules. The VE model again foresees a single oscillatory component due to longitudinal collective excitations and its spectral moments are constrained to converge up to the fourth one. Finally, a two-excitation model, labelled 2C to mean "two complex pairs" [4], is considered in those cases where also shear waves have set in in the liquid. Relaxation phenomena are represented by an effective central Lorentzian and constraints are enforced to ensure, at least, a finite fourth frequency spectral. Detailed-balance asymmetry must be applied to the above models before comparison with experiment.

2.2 Bayesian inference

As demonstrated in previous works by some of us [26,27], Bayesian methods can be successfully applied to achieve a minimally biased and probabilistically grounded modelling of experimental spectra. The inferential approach relies on the use of a Markov Chain Monte Carlo algorithm endowed with a Reversible Jump (RJ) option [28] which enables the space of free parameters to contain also the number k of excitations, and identifies the model with the highest posterior probability evaluated according to Bayes theorem, i.e., conditionally on the experimental outcome. As mentioned above, thus far the code foresees the use of simple phenomenological models for $S(Q,\omega)$, consisting of an effective central Lorentzian plus a number k of DHO doublets. Details of the Bayesian inference algorithm can be found in Ref. [26]. It is important to note that when the number of possible models (numbered by k) is a parameter itself, a Bayesian analysis naturally includes the so-called Occam's razor principle or "lex parsimoniae", which states that between two models providing an equally good account of some evidence, the one containing the lower number of parameters is always to be preferred. Thus, overparametrizations are automatically avoided within the Bayesian approach [27].

In tackling the detectability of a second (transverse) excitation in the experimental $S(Q,\omega)$, we are specially interested in the posterior distribution of the parameter k, for which we assumed a uniform prior distribution (i.e., all models are considered to be *a priori* equally probable) in order to let the inferential process be driven uniquely by the experimental evidence. An example of the results of such a statistical analysis is discussed, along with EET-based ones, in the next section.

2.3 INS and simulation results for Au and Ag

Here we summarize the main results of two investigations carried out on liquid Au [3] and Ag [4] by both INS and *ab initio* molecular dynamics (AIMD) simulations. Both metals were studied experimentally in the so-called neutron Brillouin scattering (NBS) regime, i.e., at the rather low wavevectors ranging from a few inverse nanometres (e.g., 4 nm^{-1}) to values slightly exceeding $Q_p / 2$, where $Q_p \approx 26$ nm^{-1} is the position of the maximum in the static structure factor $S(Q)$ of both metals. Since liquid metals are characterized by a high sound velocity c_s (i.e., 2568 m/s in Au and 2790 m/s in Ag) the rather energetic beam (incident energy $E_0 \approx 80$ meV, energy resolution HWHM = 1.5 meV, corresponding to 2.3 rad ps^{-1} in ω) of the small angle BRISP spectrometer at the Institut Laue Langevin (ILL) [29,30] was required to span the mentioned Q range in both cases. At the same time, the experimental work was paralleled by AIMD calculations (details are given in Refs. [3] and [4]) to check the capability of *ab initio* methods in reproducing the neutron results and, in the case of satisfactory comparisons, use the simulations to extend the study of the dynamics to higher wavevectors.

The first experiment was performed on Au. An example of the experimental $S(Q,\omega)$ at the highest Q of the measurements is given in Fig. 1.

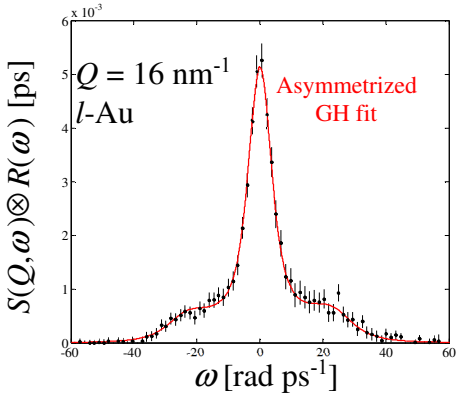

Fig. 1. Experimental (resolution broadened) $S(Q,\omega)$ of liquid Au (dots with error bars) and GH fit (red solid curve).

An EET analysis of the spectra showed that a simple GH triplet (see red curve in Fig. 1) was more than sufficient to obtain an accurate description of the data at all Q values. Thus, no evidence of transverse excitations was found from the experimental spectra of liquid Au. Nonetheless, the very good agreement between neutron data and simulations (see Fig. 2) justified an EET analysis of the simulated $S(Q,\omega)$ in the wide range 4 nm^{-1} < Q < 70 nm^{-1} probed by AIMD. In this case, a GH modelling was found to be insufficient, while spectra were perfectly described by a VE lineshape. An example of the fit quality is given in Fig. 3.

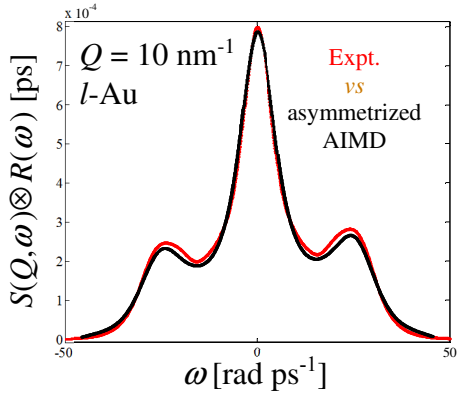

Fig. 2. Simulated $S(Q,\omega)$ at a representative Q value, taking asymmetry and experimental resolution into account (black curve). The red curve is the GH fit to the experimental data.

The VE fits to the simulations thus permitted to better resolve the central peak, but again only a single excitation could be detected. In summary, signs of shear waves turned out to be absent in both the experimental and simulated $S(Q,\omega)$ of liquid gold.

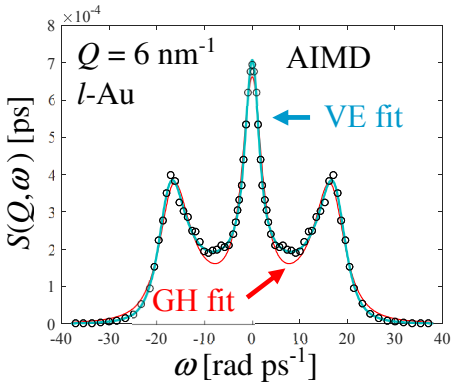

Fig. 3. Simulated $S(Q,\omega)$ of liquid Au (black circles). The GH fit (red thin curve) is clearly inaccurate, while the VE modelling (pale blue curve) provides a high fit quality.

However, shear waves clearly propagate in this liquid as witnessed by the maximum in the DoS shown in Fig. 4(b), and by the evolution, as Q grows, of a low-frequency maximum in $C_T(Q,\omega)$ (see Fig. 4(c)). The dispersion relation we were able to determine from both experiment and simulations contains instead only the longitudinal branch (Fig. 4(a)).

A study similar to that on Au was later carried out on liquid Ag, again by using the BRISP spectrometer and performing parallel AIMD calculations. As far as the measurements are concerned, a GH modelling was the only justified within the accuracy of the data (see Fig. 5), thus providing no evidence of a second excitation in the neutron spectra, like in the case of gold.

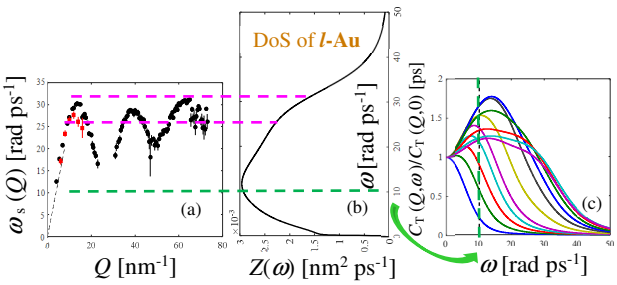

Fig. 4. (a) Dispersion relation obtained from NBS (red dots) and AIMD data (black dots); the dashed black line is the hydrodynamic law $\omega_s = c_s Q$. (b) DoS of liquid Au from AIMD. (c) Normalized $C_T(Q,\omega)$ at Q values ranging from 4.0 (blue monotonic curve) to 25.5 nm^{-1} (broad purple curve). The magenta dashed lines, containing the maxima of $\omega_s(Q)$, highlight the frequency band where the DoS shows the typical shoulder due to longitudinal modes. The green dashed curve, marking the frequency around which the maxima of $C_T(Q,\omega)$ evolve in panel (c), is shown to correspond to the frequency of the maximum in the DoS, the latter owing to the weakly dispersive transverse modes that were not detected from $S(Q,\omega)$, thereby leaving a missing branch in panel (a).

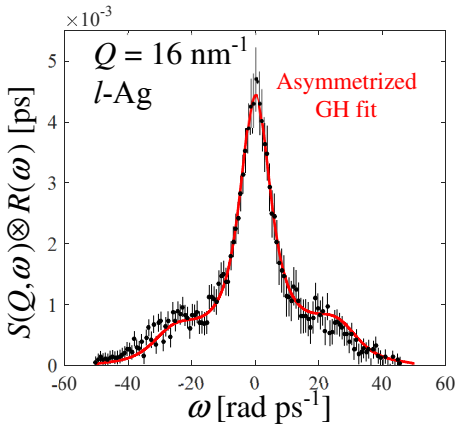

Fig. 5. Experimental (resolution broadened) $S(Q,\omega)$ of liquid Ag (dots with error bars) and GH fit (red solid curve).

By contrast, when we analyzed the AIMD simulations, we found that above Q = 15 nm^{-1} a VE lineshape became insufficient, while a 2C model (see Sect. 2.1) provided a very accurate description of the simulated spectra, as shown in Fig. 6.

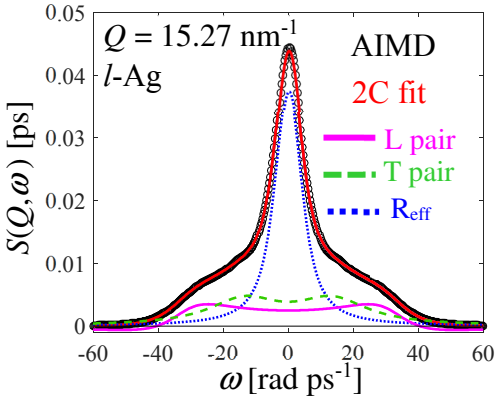

Fig. 6. AIMD $S(Q,\omega)$ of liquid Ag (circles) and 2C fit (red solid curve). The spectral components are also shown.

The 2C fits to the AIMD data of Ag thus enabled the determination of a second, low-frequency, branch $\omega_t(Q)$ in the dispersion relation displayed in Fig. 7. However, when ω_s starts to decrease, the fits become unstable and the low-frequency modes are badly determined. Conversely, transverse-like modes are clearly detected whenever ω_s and ω_t have considerably different values.

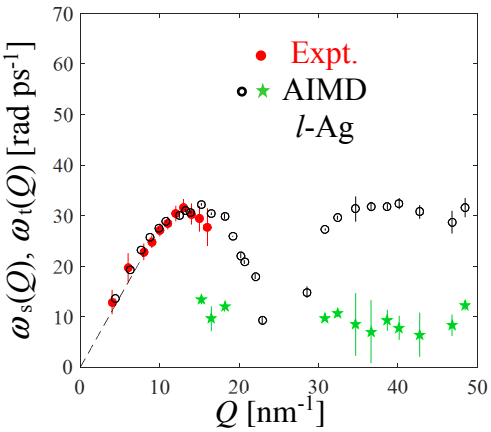

Fig. 7. Dispersion relation of liquid Ag. Red dots and black circles represent the longitudinal branch as obtained from experiment and simulations, respectively. The transverse branch (green stars) could be determined only from the AIMD results at Q values where ω_s and ω_t are sufficiently different.

Given the ambiguous situation between experimental and simulation results for liquid Ag, we revisited the neutron data by means of the second statistical route based on Bayes' theorem and briefly described in Sect. 2.2. As mentioned, we are particularly interested in the posterior distribution of the parameter k, conditional to the experimental data set at hand (globally denoted as Y). The posterior distribution of the number of excitations is reported in Fig. 8 at both low and high values of the measured Q range.

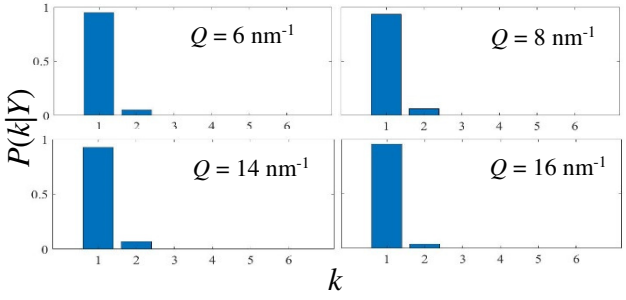

Fig. 8. Conditional posterior distributions of the number k of inelastic components in the experimental $S(Q,\omega)$ of liquid Ag at selected Q values.

Clearly, the algorithm privileges the one-excitation case, confirming the undetectability of transverse modes in the available neutron data. Moreover, very well-shaped unimodal posteriors were obtained for all the parameters [31] indicating the high reliability of the fit results which provided, within the errors, the same longitudinal dispersion curve of Fig. 7. Therefore, different ways to control the plausibility and coherence of model fitting to the data, like the EET and the Bayesian approaches, provide the same results.

To further verify the output of the inferential analysis, it is possible to switch off the RJ algorithm and check the specific posterior distributions pertaining, separately, to the $k = 1$ and $k = 2$ cases. Figure 9 shows the corresponding posterior distributions for the undamped frequency $\Omega_s = (\omega_s^2+\Gamma_s^2)^{1/2}$ of sound waves (Γ being the damping), along with that of shear waves Ω_t present only in the $k = 2$ case. It is seen that in the two-excitation case a less symmetric distribution is obtained for Ω_s and, more importantly, a broad and nearly flat distribution pertains to Ω_t. The second excitation is therefore completely undetermined, confirming the RJ-on result where k is a free parameter.

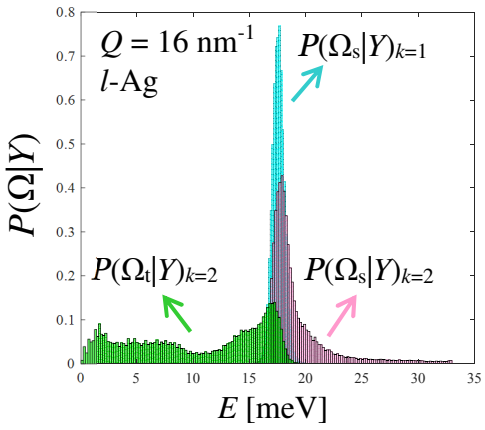

Fig. 9. Posterior distributions for the undamped frequency in the one- (cyan) and two-excitation (green for the transverse and pink for the longitudinal) cases, specifically obtained by switching off the RJ algorithm option.

Finally, to better understand why experiments did not reveal a second excitation in $S(Q,\omega)$, we performed a rather stringent test on the Ag neutron data. First, we compared the performance of the EET 2C model with the GH one of Fig. 5. Figure 10 shows that at both reported Q values the second complex pair of the 2C lineshape is characterized by a negligible amplitude.

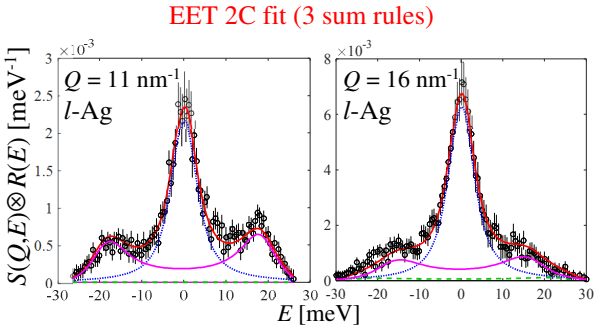

Fig. 10. Fits of the 2C lineshape to the experimental $S(Q,\omega)$ of liquid Ag. The second complex pair of the model is the dashed green curve hardly distinguishable from the zero axis.

Moreover, we found for this inelastic component an unreasonably large inelastic shift and an error on the damping doubling the damping value itself, meaning that such a parameter is undetermined. Therefore, according to *lex parsimoniae*, there are no reasons to choose the 2C result (8 parameters) in place of the GH

one (5 parameters) which provides an identical global fit curve.

Then, we analyzed the neutron spectra in the phenomenological fashion adopted in other works [18,19], without any constraint except normalization. Figure 11 puts in evidence quite an embarassing situation, resembling very much that of Fig. 1 of Ref. [18] or of Ref. [19].

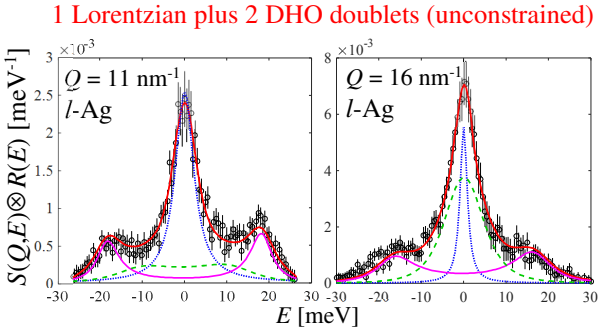

Fig. 11. Fits of the neutron data on liquid Ag using the unconstrained phenomenological model specified in the figure title.

The previous example demonstrates that the use of constrained models (i.e., obeying at least the most important sum rules) can completely change the results and the deduced physical properties. Indeed, uncontrolled fit procedures, escaping either physical or statistical consistency criteria are likely prone to biases of confirmation. Moreover, the above test shows that the undetectability of low-frequency contributions in appropriate modellings of the experimental $S(Q,\omega)$ is not due to the limited resolution or to the scattering of the data-points, but is merely *a matter of analysis*.

As a final remark regarding this discussion on high-temperature classical fluids, we can conclude that the experimental observation of shear waves is not yet assessed for either system, and still remains out of reach of the present spectroscopic techniques. In fact, convincing indications that $S(Q,\omega)$ bears also the signature of the transverse dynamics were only found by means of rather recent, quantitative EET-studies of simulation results [4]. On the other hand, neutron data on these classical systems showed the effectiveness of *ab initio* simulation methods, which open the way to extended investigations of the dynamical behaviour of simple classical liquids, without limitations in wavevector.

3 "Boltzmann" quantum liquids: D_2

Liquid hydrogen and deuterium represent an intermediate case within the few systems displaying quantum behaviour (He, H_2, D_2, and Ne). In fact, they are so-called Boltzmann quantum fluids, where, differently from the case of helium, exchange effects due to particle indistinguishability are supposed to be negligible in comparison to particle delocalization, and Boltzmann statistics can still be assumed to hold. Therefore, distinct trajectories in phase space can still be defined, and molecular dynamics methods applied, although with obvious differences from a purely classical treatment. This is the reason why H_2 and D_2, can be considered as *moderate* quantum fluids, since only single-molecule delocalization is actually responsible for a nonclassical behaviour, as suggested by the limited values [32] reached by the de Broglie thermal wavelength $\Lambda = h / (2\pi M k_B T)^{1/2}$ even close to their respective triple points.

The characteristic length scale considered for comparisons with Λ at a certain temperature is the mean interparticle distance $l = n^{-1/3}$, with n being the number density. At all relevant liquid densities and temperatures of H_2 and D_2, the condition $\Lambda < l$ holds [32], implying that overlap of the spatial wave functions of two adjacent molecules, and consequently quantum exchange, does not occur on average, so that quantum statistics need not be invoked. Nonetheless, Λ can reach values of the order of the molecular size, giving anyway rise to quantum delocalization effects that must be accounted for in some approximate, semiclassical way.

A recent review of the available semiclassical approximations for calculations of the dynamic structure factor of moderate quantum fluids, like RPMD [15], FK-Linearized Path Integral (LPI) [16] and FK-Quasi Classical Wigner (QCW) [17], can be found in Ref. [14].

On the experimental side, neutron measurements on these liquids have been few, and often reporting the double differential cross section in arbitrary units (including the rotational contributions) [12,13] rather than the centre of mass dynamic structure factor $S_{CM}(Q,\omega)$ in absolute ones. Experimental knowledge of the translational dynamics would instead be very helpful for an in-depth verification of the mentioned simulation methods, enabling or not their possible use in applications. These reasons induced us to perform a neutron measurement on liquid D_2, accompanied by the RPMD, FK-LPI and FK-QCW calculations detailed in Ref. [14], all relying on the isotropic Silvera and Goldman intermolecular potential [33].

The experiment was carried out on the BRISP spectrometer in the standard configuration used also for the metallic samples. After corrections for background, attenuation and multiple scattering, the single scattering intensity of a diatomic homonuclear molecule can be schematized as

$$I^{(1)}(Q,E) = C\,\{(k_1/k_0)\,[u(Q)S_{CM}(Q,E)+J(Q,E)]\}\otimes R(E), \quad (6)$$

where C is a normalization factor and k_1/k_0 is the ratio of scattered to incident neutron wavevector. In Eq. (6), $u(Q)$ is the intermolecular cross section depending only on the coherent scattering length of D, while $J(Q,E)$ is an intramolecular term accounting for the rotational structure and which depends also on the incoherent scattering length of D. Both $u(Q)$ and $J(Q,E)$ can be confidently calculated within well-known approximations complying, in the case of $J(Q,E)$, with the asymmetry requirements of quantum spectra [14]. Finally, $R(E)$ is the instrument energy resolution function.

The quantity we are interested in is the quantum $S_{CM}(Q,E)$, which is related to the Kubo (symmetric) dynamic structure factor $S_{CM,K}(Q,E)$ through the well-

know asymmetry factor $\beta E / [1-\exp(-\beta E)]$, with $\beta = (k_B T)^{-1}$. Therefore, one can model $S_{CM,K}(Q,E)$ by means of a classical lineshape and perform an overall fit to $I^{(1)}(Q,E)$ according to Eq. (6) and to the asymmetry condition quoted above. Again, a GH model for $S_{CM,K}(Q,E)$ was found to provide an accurate description of the data, as shown in Fig. 12(a) for a representative Q value. The various components of the fit function can be better appreciated in the zoom of Fig. 12(b) and are detailed in the caption.

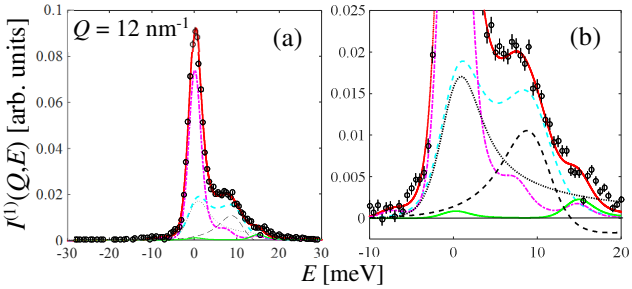

Fig. 12. (a) Single scattering intensity of liquid D_2 (black circles with error bars) and global fit curve (red solid line) according to Eq. (6). (b) Zoom of panel (a): the magenta dot-dashed curve is the intramolecular component, with visible rotational lines; the dotted and dashed black curves are the elastic and inelastic components which sum up to give, within a normalization factor, the asymmetric GH-based $S_{CM}(Q,E)$ (cyan dashed curve); the green solid curve accounts for a small amount of H_2 likely present in the sample.

The fits to $I^{(1)}(Q,E)$ then provided the sought-for absolute scale and resolution-free $S_{CM}(Q,E)$. The latter is compared, at 9 nm^{-1}, with the various simulation results in Fig. 13. Similar results were obtained at other wavevectors [14].

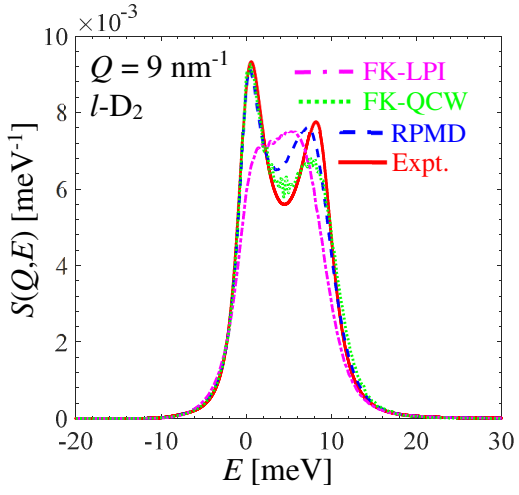

Fig. 13. Resolution-free quantum dynamic structure factor of liquid D_2 in absolute units, as obtained from the fits to the neutron data (red solid curve) and from different semiclassical approximations used in available quantum simulation techniques, each one specified in the legend and detailed in Ref. [14].

The comparisons in Fig. 13, needless to say, are quite unsatisfactory independently of the attempted simulation method. Neutron data visibly show much more marked collective excitations. Moreover, simulations do not agree even among themselves. Despite the clear loss of important details of the dynamical structure, it is anyway valuable that the absolute scale of neutron and simulation data is the same.

In order to compare frequencies and damping coefficients derived from experiment and simulations in more detail, we carried out also a thorough EET analysis of the RPMD and FK-QCW results. All simulation outputs were found to be accurately described by a VE model at the investigated Q values. The corresponding longitudinal dispersion curve and wavevector dependence of the damping coefficient of liquid D_2, are finally shown in Fig. 14.

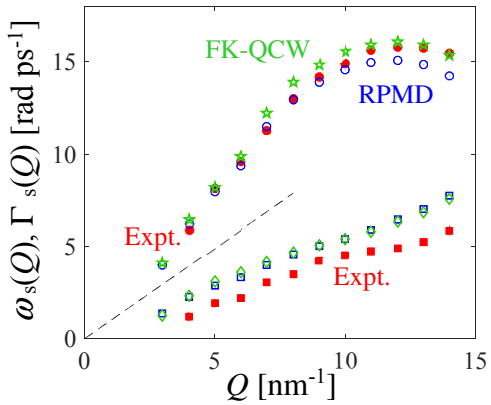

Fig. 14. Experimental (red full circles), RPMD (blue empty circles), and FK-QCW (green empty stars) dispersion curve of sound modes. The dashed black line is the hydrodynamic behaviour $c_s Q$, with $c_s = 0.984$ nm/ps. The damping coefficient is displayed with red full squares, blue empty squares, and green empty diamonds for experiment, RPMD and FK-QCW, respectively.

Figure 14 shows that, although the dispersion curves do not agree within the errors at some Q value, this property is reasonably captured by simulations, especially by the FK one. Conversely, the striking feature in the plot is the smaller damping deduced from the measurements.

The long lifetime of collective excitations is considered to be one of the main dynamical manifestations of quantum behaviour [34]. Apparently, the present simulation techniques do not fully grasp a salient feature of quantum liquids dynamics. Of course, we cannot exclude with absolute certainty some systematic errors in the (demanding) neutron data analysis. However, the disagreement among simulation results suggests that the semiclassical approximations adopted in each technique should anyway be improved. Indeed, while the dispersion curve is acceptably accounted for by computations, which is anyway an achievement, an important property of cold liquids, i.e., the damping of sound waves, is largely missed and systematically overestimated.

4 Final remarks

The examples reported in this work show that the degree of accuracy with which simulations of $S(Q,\omega)$ are able to reproduce experimental data is very different for classical and quantum liquids: it is very high in the first case and still rather low in the second.

As a general result, we demonstrated that unconstrained analyses of $S(Q,\omega)$ can be deceptive, while use of the EET enables very accurate and physically-grounded descriptions of both experimental and simulation data.

The future of course lies in the implementation of EET-based models within algorithms exploiting Bayesian inference, so to maximize both physical and statistical consistency of fit results and avert possible biases in the analysis.

We acknowledge the BRISP spectrometer at the ILL, no longer operational, which was the state of the art instrument for neutron Brillouin scattering at thermal energies: a neutron technique of extreme importance for studies of dense liquids dynamics. Regretfully, no equivalent instrument exists at present in the world, which is a deadweight loss.

References

1. J. R. D. Copley and J. M. Rowe, Phys. Rev. Lett. **32**, 49 (1974).
2. O. Söderström, J. R. D. Copley, J.-B. Suck, B. Dorner, J. Phys. F: Metal Phys. **10**, L151 (1980).
3. E. Guarini *et al.*, Phys. Rev. B **88**, 104201 (2013) and references therein.
4. E. Guarini *et al.*, Phys. Rev. B **102**, 054210 (2020).
5. U. Balucani and M. Zoppi, Dynamics of the Liquid State (Clarendon, Oxford, 1994).
6. Chr. Morkel, Chr. Gronemeyer, W. Gläser, J. Bosse, Phys. Rev. Lett. **58**, 1873 (1987).
7. C. Morkel and C. Gronemeyer, Z. Phys. B **72**, 433 (1988).
8. P. Verkerk, J. Westerweel, U. Bafile, L. A. de Graaf, W. Montfrooij, I. M. de Schepper, Phys. Rev. A **40**, 2860 (1989).
9. M. Celli *et al.*, Phys. Rev. B **84**, 140510 (2011).
10. M. Zoppi, D. Colognesi, M. Celli, Eur. Phys. J. B **23**, 171 (2001).
11. E. Guarini *et al.*, Phys. Rev. B **93**, 224302 (2016).
12. F. J. Bermejo *et al.*, Phys. Rev. B **47**, 15097 (1993).
13. F. J. Bermejo *et al.*, Phys. Rev. Lett. **84**, 5359 (2000).
14. E. Guarini *et al.*, Phys. Rev. B **104**, 174204 (2021).
15. I. R. Craig and D. E. Manolopoulos, J. Chem. Phys. **121**, 3368 (2004).
16. J. A. Poulsen, G. Nyman, P. J. Rossky, J. Chem. Phys. **119**, 12179 (2003).
17. K. K. G. Smith, J. A. Poulsen, G. Nyman, P. J. Rossky, J. Chem. Phys. **142**, 244112 (2015).
18. S. Hosokawa *et al.*, Phys. Rev. Lett. **102**, 105502 (2009).
19. V. M. Giordano and G. Monaco, PNAS **107**, 21985 (2010).
20. D. Levesque, L. Verlet, J. Kürkijarvi, Phys. Rev. A **7**, 1690 (1973).
21. J.-B. Suck, Cond. Matter Phys. **11**, 7 (2008).
22. U. Bafile, E. Guarini, F. Barocchi, Phys. Rev. E **73**, 061203 (2006).
23. F. Barocchi, U. Bafile, M. Sampoli, Phys. Rev E **85**, 022102 (2012).
24. F. Barocchi and U. Bafile, Phys. Rev E **87**, 062133 (2013).
25. F. Barocchi, E. Guarini, U. Bafile, Phys. Rev E **90**, 032106 (2014).
26. A. De Francesco, E. Guarini, U. Bafile, F. Formisano, L. Scaccia, Phys. Rev. E **94**, 023305 (2016).
27. A. De Francesco, A. Cunsolo, L. Scaccia, Bayesian approach for X-ray and neutron spectroscopy. In *Inelastic X-ray scattering and X-ray Powder Diffraction Applications* (Chap. 2) 26 (IntechOpen 2020).
28. P. J. Green, Biometrika **82**, 711 (1995).
29. D. Aisa *et al.*, Nucl. Instr. Meth. A **544**, 620 (2005).
30. D. Aisa *et al.*, J. Non-cryst. Solids **352**, 5130 (2006).
31. A. De Francesco, U. Bafile, A. Cunsolo, L. Scaccia, E. Guarini, Sci. Rep. **11**, 13974 (2021).
32. M. Zoppi, M. Celli, A. K. Soper, Phys. Rev. B **58**, 11905 (1998).
33. I. F. Silvera and V. V. Goldman, J. Chem. Phys. **69**, 4209 (1978).
34. H. H. Glyde, Excitations in Liquid and Solid Helium, (Clarendon Press, Oxford, 1995).